Biaxial Mechanical Properties of the Native and Glutaraldehyde-Treated Aortic Valve Cusp: Part II—A Structural Constitutive Model

Kristen L. Billiar[1]
Department of Biomedical Engineering,
University of Miami,
Coral Gables, FL 33124

Michael S. Sacks[2]
Department of Bioengineering,
University of Pittsburgh,
Pittsburgh, PA 15261

We have formulated the first constitutive model to describe the complete measured planar biaxial stress–strain relationship of the native and glutaraldehyde-treated aortic valve cusp using a structurally guided approach. When applied to native, zero-pressure fixed, and low-pressure fixed cusps, only three parameters were needed to simulate fully the highly anisotropic, and nonlinear in-plane biaxial mechanical behavior. Differences in the behavior of the native and zero- and low-pressure fixed cusps were found to be primarily due to changes in the effective fiber stress–strain behavior. Further, the model was able to account for the effects of small (<10 deg) misalignments in the cuspal specimens with respect to the biaxial test axes that increased the accuracy of the model material parameters. Although based upon a simplified cuspal structure, the model underscored the role of the angular orientation of the fibers that completely accounted for extreme mechanical anisotropy and pronounced axial coupling. Knowledge of the mechanics of the aortic cusp derived from this model may aid in the understanding of fatigue damage in bioprosthetic heart valves and, potentially, lay the groundwork for the design of tissue-engineered scaffolds for replacement heart valves. [S0148-0731(00)00504-5]

Introduction

An understanding of the mechanics of the native aortic valve (AV) cusp and the changes that occur due to chemical treatment are needed to establish an improved understanding of native valve function and to clarify the mechanisms of poor porcine bioprosthetic heart valve (PBHV) durability. Constitutive models can also guide tissue engineering technologies by forming the basis for rational engineering of biological prosthetic heart valve biomaterials. Further, accurate constitutive models are required for computational stress analysis of the AV cusp, which could provide a powerful design tool by integrating valve geometry, tissue mechanical properties and structure, and solid–fluid coupling (e.g., [1,2]). Surprisingly, constitutive models for the aortic valve cusp do not exist.

Most previous work on the mechanical properties of the native and chemically treated AV has relied on uniaxial mechanical testing [3–5]. These studies demonstrate that chemical fixation of intact valves, especially under pressure, alters the mechanical properties of the cusps. Marked decreases in the extensibility are generally attributed to ''locking'' the collagen fibers in the uncrimped state [6–8]. Tests on thin tissue strips however, cannot mimic the heterogeneous multi-axial deformation fields, combined loading sequences, and native fiber kinematics found in the physiological environment. Mayne et al. [9] and Christie et al. [10] have performed equibiaxial testing (i.e., equal levels of tension applied to each test axis) that overcomes many of the above-described limitations of uniaxial loading. However, derivation of a constitutive relationship solely from equibiaxial test data is limited due to multiple collinearities that confound the ability to obtain reliable, unique model parameter values [11].

In Part I of this work, we developed experimental techniques for biaxial mechanical testing of the AV cusp and applied these techniques to characterize the biaxial mechanical response of native and glutaraldehyde-treated porcine AV cusps [12]. Since the physiological fiber kinematics were preserved under biaxial stress, the circumferential and radial strains were smaller under biaxial loading than those reported for uniaxial loading (e.g., [4,13,14]). In fact, the coupling between testing axes was so strong that the slope of the circumferential stress–strain curve was often negative even in the equibiaxial protocol despite the presence of equal tension on each axis. This behavior was also noted by Mayne et al. [9], but could not be explained. Clearly, a constitutive model is needed to truly understand the aortic cusp behavior and its implications on the mechanics of the intact valve.

In the present work, we formulate a constitutive model guided by the fibrous structure of the aortic valve cusp to describe its in-plane biaxial mechanical properties using the experimental data from Part I of this study [12]. The model separates the properties of the fibers from their geometric configuration by employing a fiber angular distribution. The model includes the effects of shear strains, as they can be significant when biaxial testing highly aligned fibrous connective tissues [12]. Multiple biaxial protocols were simultaneously fit and the predictive capability of the model verified by using experimental data not used in the fit. We demonstrate that only three parameters are needed to describe completely the measured in-plane biaxial quasi-static response of the AV cuspal tissue.

Methods

Experimental Database. The methods for biaxial testing of aortic heart valve cusps and the general mechanical behavior of native and 0.625 percent aqueous glutaraldehyde (GL) low-pressure (0.5 kPa, 4 mmHg) treated cusps have been previously

[1]Current address: Organogenesis, Inc., 150 Dan Rd., Canton, MA 02021.
[2]Corresponding author.

Contributed by the Bioengineering Division for publication in the JOURNAL OF BIOMECHANICAL ENGINEERING. Manuscript received by the Bioengineering Division May 25, 1999; revised manuscript received March 22, 2000. Associate Technical Editor: L. A. Taber.

described in Part I [12]. Briefly, one square specimen was cut from each cusp, marked with graphite markers, submerged in isotonic saline, and connected to the biaxial apparatus with the tissue axes approximately aligned to the biaxial testing device axes. The complete biaxial testing protocol consisted of the following seven Lagrangian membrane stress (T_{ij}) controlled protocols: $T_{11}:T_{22}=10:60$, 30:60, 45:60, 60:60, 60:45, 60:30, and 60:2.5 (N/m). Here, the subscripts 1 and 2 correspond to the circumferential and radial directions of the cusp, respectively. The in-plane deformation gradient tensor F_{ij} was computed from the marker displacements, with physical components $F_{11}=\lambda_1$, $F_{12}=\kappa_1$ $F_{21}=\kappa_2$, $F_{22}=\lambda_2$ (Appendix 1). The components of the membrane stress were calculated as $T_{11}=P_1/w_2$, $T_{22}=P_2/w_1$, $T_{12}=T_{21}=0$, where P_i and w_i were the axial load and side width, respectively ($i=1,2$). The data were then thinned to a total of ~400 data points (200 per axis) for each specimen to decrease the time required for numerical operations.

In addition to the Part I specimen database, we also present results from glutaraldehyde treated valves chemically treated under zero trans-valvular pressure. Contemporary PBHV are typically chemically treated under 2–4 mmHg trans-valvular pressure in order to maintain proper cuspal geometry. We have shown that rapid and profound changes in the collagen fiber crimp occur between 0 and 4 mmHg [15]. Thus, by using PBHV prepared under zero trans-valvular pressure we can determine the effects of alterations in the collagen fiber crimp on the effective fiber stress–strain properties, independent of other chemical treatment or related valve design changes.

General Considerations in Formulating the Constitutive Model. Due to the highly nonlinear, large deformation response of soft tissues, there exists no unique form of the phenomenological constitutive model. Classic approaches to define the constitutive model typically determine the model form through examination the stress–strain relationship under a variety of loading conditions. The location of the material axes is guided by gross observations of the structure of the tissue (e.g., fiber directions). The chosen constitutive model is then verified by the goodness of fit, predictive capabilities, and numerical stability of the model parameters (see Chap. 7 in Fung [16] for an excellent review). Techniques developed by Humphrey et al. [17,18] attempt to derive the specific fundamental form of the constitutive relationship directly from the experimental data. This technique has also been used successfully for the mitral valve tissue leaflet [19].

While phenomenological constitutive models are able to fit the mechanical data well, they are limited in that they cannot elucidate the underlying cause of mechanical behavior. Alternatively, structurally based constitutive models not only avoid ambiguities in material characterization but also offer insights into the function, structure, and mechanics of tissue components. The fiber architecture [15] and biaxial mechanical data [12] suggest that a structural approach is the most suitable method for the formulation of a constitutive model for the AV cusp. For example, in Part I of this work, we demonstrated that strong axial coupling produced nonmonotonic relationships between stress and strain, including negative strains [12]. Our related work on native and chemically treated bovine pericardium suggests that a structural approach is both feasible and attractive for bioprosthetic heart valve biomaterials [20,21].

Specialization of the Structural Model Derivation for the AV Cusp. The constitutive model for the aortic valve cusp presented herein is based on work by Lanir [22,23] for the homogeneous biaxial deformation of planar fibrous tissues. The formulation is founded on the basic assumption that the gross behavior of the tissue results from the collective contribution of the individual components. External loads are assumed to be resisted by the extensional strain energy of the fibers alone, i.e., compressive stiffness and bending rigidity are assumed to be negligible. The mechanical contribution of the ground matrix (including the hydrostatic pressure) appears to have a negligible impact on the pseudoelastic response [23–25]. Although the cusp exhibits marked viscoelastic effects at high strain rates [3,4,26] in addition to slight hysteresis, in the range of loading rates employed for our biaxial tests the stress–strain response is negligibly altered by viscoelastic effects [27]. Thus, in the development of the present model time-dependent effects are ignored and only the pseudoelastic loading response is considered.

To achieve the combination of low flexural rigidity necessary to allow normal valve opening with minimal resistance to flow and high tensile strength required to resist trans-valvular pressures in excess of 80 mmHg, the AV cusp has evolved into highly specialized trilayered cuspal structure. These layers, the ventricularis, spongiosa, and fibrosa, vary in thickness, structure, and composition [28]. As its name implies, the ventricularis layer faces the left ventricular chamber and is composed of a dense network of collagen and elastin fibers. The spongiosa layer contains a high concentration of proteoglycans and presumably acts as lubrication between the fibrous layers. The fibrosa layer is composed predominantly of a dense network of collagen fibers, which form thick cords coursing in the circumferential direction, and is thought to be the major stress-bearing layer.

Although each layer undoubtedly plays an important role in the function of the cusp, detailed modeling of this trilayered structure would be highly complex. Tensile loads are carried primarily by the collagen fibers that form the thick chordal structures of the fibrosa. Elastin, found mainly in the ventricularis, plays a secondary role in resisting planar biaxial loads and is more important in returning the cusp to its unloaded shape. Thus, we assume that the cusp can be modeled as a single layered tissue composed of a single fiber type. Since the collagen fiber crimp distribution in the cusp is difficult to quantity and highly variable [8], we choose only to simulate the ''effective'' fiber stress–strain properties. We have chosen the following exponential stress–strain law to model the effective fiber stress–strain law:

$$S_f=A[\exp(BE_f)-1] \tag{1}$$

where S_f is the second Piola–Kirchoff fiber stress, E_f is the fiber Green's strain computed using $E_f=0.5(\lambda_f^2-1)$ where λ_f is the fiber stretch ratio. This formulation avoids detailed descriptions of fiber interactions and complex crimp distributions.

For valvular tissue, it is convenient to work with membrane tensions (i.e., force/unit length) due to considerations such as variable tissue thicknesses and heterogeneous layer structures, both of which result in unknown nonuniform transmural stress distributions [12]. These considerations lead us to adopt Lagrangian membrane tension (force/unloaded unit length) when performing the biaxial tests and in the formulation of the constitutive relation.

When using membrane tension with this fibrous tissue, we must consider the effects of interspecimen variations in the cusp thickness, h, and fiber volume fraction, V_f. Both parameters will affect the total number of fibers but are virtually impossible to quantify throughout each specimen. Examination of representative histological slides indicated that lower thickness generally corresponds to a fiber higher volume fraction. Likewise, our biaxial mechanical experimental data for the valve [12] indicated that under equibiaxial tension, the peaks strains are relatively uniform within any given specimen group. These observations suggest that the total number of loaded fibers within each cusp does not vary considerably, and we can assume that the total number of loaded fibers remains relatively constant between specimens. Thus, the product hV_f can be conveniently absorbed into the material constant A in Eq. (1), resulting in the following expression for the Lagrangian fiber membrane tensions

$$T_f=\lambda_f S_f^*=\lambda_f A^*[\exp(BE_f)-1] \tag{2}$$

where $A^*=hV_fA$. Note that in Eq. (2) we use the relation $T_f=\lambda_f S_f^*$ since the loading on each fiber is considered uniaxial, with T_f expressed in units of force/unit length.

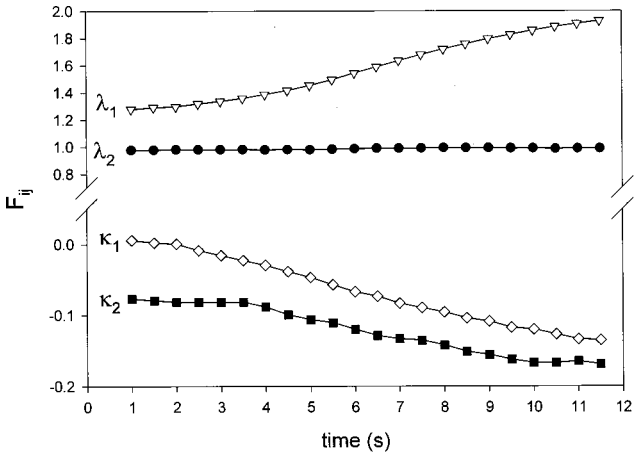

Fig. 1 Representative response of the components of deformation gradient tensor F_{ij} (λ_1, κ_1, κ_2, and λ_2, where subscripts 1 and 2 correspond to the circumferential and radial axes, respectively) during the loading phase of a biaxial test. Note the significant in-plane shear values (κ_1 and κ_2), which are plotted using a different scale.

Based on previous measurements in our laboratory [29], as a first approximation, the kinematics of the AV cusp can be assumed to follow an affine rule, i.e., the fiber strain can be computed from the tensorial transformation of the global strain tensor to the local fiber coordinates. Further, as noted in Part I [12] the deformation in the strain measurement area was found to be acceptably homogeneous. Thus, the stretch along a fiber oriented at an angle θ with respect to the X_1 (or circumferential) biaxial testing device axis is given by

$$\lambda_f^2=[(\lambda_1^2+\kappa_2^2)\cos^2\theta+2(\lambda_1\kappa_1+\lambda_2\kappa_2)\cos\theta\sin\theta + (\lambda_2^2+\kappa_1^2)\sin^2\theta] \tag{3}$$

In our biaxial experiments, the external loads are applied along the biaxial testing apparatus axes, X_1 and X_2, and the sides of the tissue sample are perpendicular to the axes in the undeformed state. When an external load is applied to the tissue the fibers stretch and rotate from their original angle, θ, to a final angle, β, which is a function of the deformation gradient, **F**, the original fiber angle θ, and the kinematics of the fibers. The fiber stress is directed along the axis of the fiber with unit vector $\vec{s}=\cos\beta\vec{i}+\sin\beta\vec{j}$ where

$$\cos\beta=\frac{(\lambda_1\cos\theta+\kappa_1\sin\theta)}{\lambda_f} \qquad \sin\beta=\frac{(\kappa_2\cos\theta+\lambda_2\sin\theta)}{\lambda_f} \tag{4}$$

The unique design of our biaxial device allows in-plane shear [30], which is significant in many of the cusp specimens (Fig. 1). Thus, the kinematic relationships stated in Eq. (4) must include both normal and in-plane shearing strains. Equilibrium force balance yields the following relationships for the Lagrangian membrane stresses along the test axes:

$$T_{11}=\int_{-\pi/2}^{\pi/2}T_f(E_f)R(\theta)\cos\theta\cos\beta d\theta \qquad T_{22}=\int_{-\pi/2}^{\pi/2}T_f(E_f)R(\theta)\sin\theta\sin\beta d\theta \tag{5}$$

where $R(\theta)$ is the angular distribution of the fibers with respect to the X_1 or circumferential axis.

Substituting in the equations for T_f (Eq. (2)), λ_f (Eq. (3)), and $\sin\beta$ and $\cos\beta$ (Eq. (4)) into Eq. (5) yields the following relationships for the Lagrangian membrane stresses along the test axes:

$$T_{11}=\int_{-\pi/2}^{\pi/2}S_f^*(E_f)R(\theta)(\lambda_1\cos^2\theta+\kappa_2\sin\theta\cos\theta)d\theta \qquad T_{22}=\int_{-\pi/2}^{\pi/2}S_f^*(E_f)R(\theta)(\lambda_2\sin^2\theta+\kappa_1\sin\theta\cos\theta)d\theta \tag{6}$$

Equation (6) represents the final form of the structural constitutive model used in the present study. The equations reduce to those used by Lanir et al. [31] and Zioupos and Barbenel [32] if the shear and rotation are neglected (i.e., $\kappa_1=\kappa_2=0$).

Form of the Angular Fiber Distribution, $R(\theta)$. Based on our small angle light scattering (SALS) results for the AV cusp [15], we assume that $R(\theta)$ follows a Gaussian distribution given by:

$$R(\theta)=\frac{1}{\sigma\sqrt{2\pi}}\exp\left[\frac{-(\theta-\mu)^2}{2\sigma^2}\right] \tag{7}$$

where σ is the standard deviation and μ is the mean of the distribution. SALS results have indicated that the fiber distribution in the belly region of the cusp can be consistently represented with $\sigma=\sim35$ deg [15]. However, since the AV cusp is not composed of a single population of collagen fibers, different fiber populations within the cusp may experience different loading in vivo (see Discussion). Thus, we did not directly utilize the SALS data for $R(\theta)$ as done previously for native and chemically treated bovine pericardium [20], but utilized Eq. (7) to represent $R(\theta)$. We instead used SALS only to measure μ, as discussed below, assuming that the populations have the same preferred direction.

In the present structural model formulation (Eq. (6)), σ is treated as an independent parameter, resulting in a total of three parameters, A^*, B, and σ. The parameter μ was determined experimentally for each specimen by using the preferred fiber directions as determined by SALS [15]. Briefly, the fiber architecture of the area delimited by the graphite markers of each specimen was determined using SALS, and the value for μ taken to be the mean preferred fiber direction. The samples were rotated and deformed to some extent when removed from the biaxial apparatus and mounted on the SALS machine. This rotation was quantified by comparing the marker positions relative to the SALS device axes with the marker positions relative to the biaxial testing device axes. The SALS marker position were considered to be the positions of the biaxial markers following a general two-dimensional deformation required to mount the specimen in the scanning well and position it relative to the SALS device axes. This rotation was removed using polar decomposition to separate the effects of rigid body rotation (due to misalignment in the SALS device) and deformation (Appendix 2 and [33]). In addition, the use of the particular form of Eq. (7) had the advantage of allowing the determination of the structural model's sensitivity to σ and μ.

Parameter Estimation. To estimate the parameters A^*, B, and σ, a direction set method based on Powell's quadratically convergent method [34] was used to minimize the objective function

$$\Phi=\sum_k\ (T_{11}^k-\overline{T}_{11}^k)^2+(T_{22}^k-\overline{T}_{22}^k)^2 \tag{8}$$

where T_{ij}^k are the estimated tension values and $\overline{T}_{ij}^k$ are the measured tensions evaluated for the kth data point. In the current study k ranges over the data sets from protocols 2 through 6 (see [12]). The ''outer'' protocols (1 and 7) with the largest and smallest tension ratios ($T_{11}:T_{22}$) were not used for the estimation of ma-

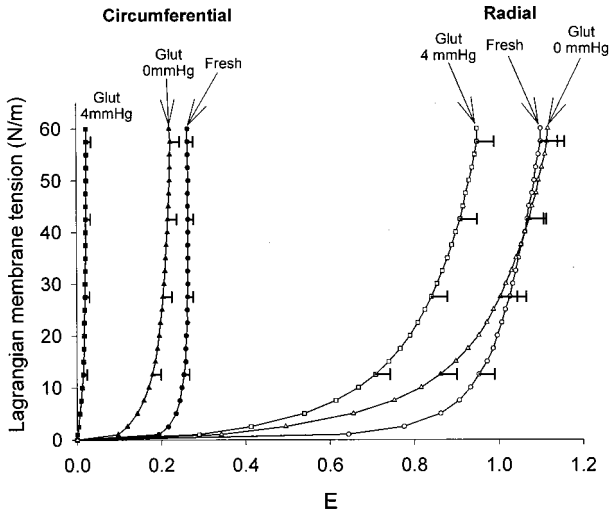

Fig. 2 Mean stress–strain response of the AV cusps under equibiaxial tension for the native and 0 and 4 mmHg glutaraldehyde-treated tissue. Note the difference in the biaxial response between the 0 and 4 mmHg demonstrating how the state of collagen fiber crimp during fixation can influence the mechanical response.

terial parameters. Instead, the data from these protocols were used to check how well the model predicted the material behavior in these extreme protocols. Although fewer protocols could have been used for the fit, the stability of the parameters was maximized by sampling over as large a domain as possible [11,17,35,36]. Since expressions for the membrane tensions (Eq. (6)) are coupled, the data from both axes were fit simultaneously. Also, since the fibers were assumed to have negligible bending and compressive stiffness, the stress from fibers with negative strains was neglected.

As the parameter estimation was nonlinear, the existence of multiple minima could not be excluded. Nine different combinations of initial parameters were used for each specimen and the contour plots of the error surface were studied to assure that the solutions were ''well behaved,'' i.e., no saddle points existed and the global minimum error for each sample was found. The sensitivity of the parameter estimation to experimental error was also examined by superimposing various levels of ''Gaussian noise'' on a set of synthetic data. As expected, the error increased monotonically with the amplitude of noise; however, the parameter values themselves were affected only slightly [37].

Results

Effects of Zero-Pressure Fixation. In addition to native (nonfixed) and low-pressure fixed AV cusps, the experimental data generated for this study included previously unpublished data for zero-pressure fixed AV cusps. Results from this new set indicated that the biaxial mechanical response was very similar to the native tissue (Fig. 2). The main effect of the zero-pressure fixation state is an increase in compliance along both stretch axes compared to the 4 mmHg fixed state. This result is consistent with similar studies by Mayne et al. [9]. This result clearly demonstrates the profound effects that the collagen crimp state during fixation have on the resulting biaxial mechanical properties (see Discussion).

General Model Fitting Capabilities. The fit of the model to the data was good despite the complexity of the mechanical response over the broad range of both tissue preparation and biaxial loading states (Fig. 3). The model fit the data from all seven protocols well even though the data from the outer protocols (1 and 7) were not used in the parameter estimation. The optimal parameters for each specimen, the residual root mean square error of the fit, Rrms, and the coefficient of determination, r^2, are listed

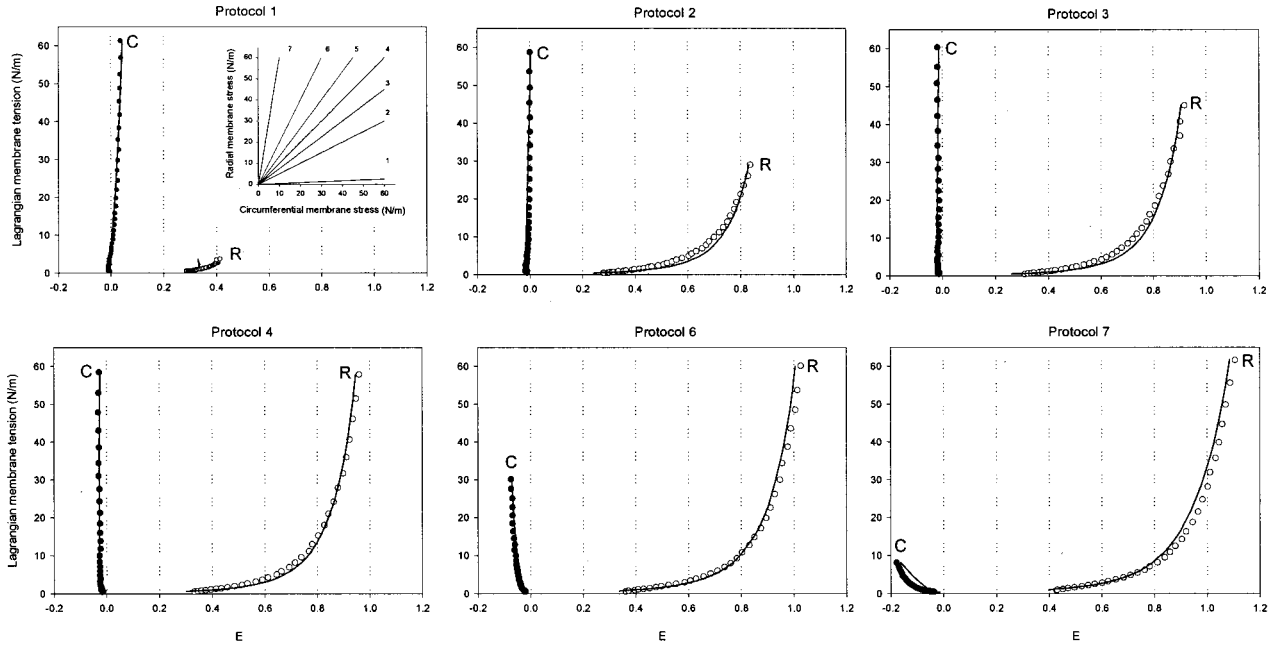

Fig. 3 Stress–strain curves for six of the seven loading protocols for a 4 mmHg fixed specimen (open circles) and the simulated stress–strain curves (lines) using the optimal parameters (Table 1). The structural constitutive model demonstrated an excellent fit to the data, including the presence of large negative circumferential strains due to strong axial coupling. Although protocol five was not shown for clarity of presentation, it also demonstrated an equally good agreement between theory and experiment. Inset: biaxial testing protocols with the corresponding protocol numbers shown for reference.

Table 1 Structural model fit parameters for the native AV and PBHV cusp

NATIVE	A* (N/m)	B	σ (deg)	Rrms (N/m)	r^2
1	0.0071	21.9	15.5	7.0	0.974
2	0.0042	20.8	11.4	9.9	0.967
3	0.0589	18.3	9.3	6.7	0.929
4	0.0042	29.8	10.1	5.4	0.938
5	0.1585	19.5	12.9	11.2	0.928
6	0.0053	28.1	11.2	12.2	0.939
7	0.0876	17.3	11.6	9.4	0.971
8	0.0068	25.5	13.0	10.2	0.940
9	0.0729	22.4	10.5	10.9	0.963
10	0.0208	23.2	11.1	8.3	0.897
11	0.1608	19.8	10.7	7.7	0.950
mean	0.05	22.4	11.6	9.0	0.95
sem	0.02	1.2	0.5	0.6	0.01

0 mmHg	A* (N/m)	B	σ (deg)	Rrms (N/m)	r^2
1	2.080	11.3	17.6	3.4	0.975
2	1.390	11.7	16.5	2.5	0.984
3	0.950	14.8	14.4	4.0	0.965
4	0.870	10.8	18.3	5.8	0.929
5	0.390	12.1	17.1	3.2	0.976
6	1.760	10.6	13.0	4.0	0.963
7	1.700	11.1	13.4	3.2	0.980
8	0.730	11.0	18.9	3.3	0.974
mean	1.23	11.7	16.1	3.7	0.97
sem	0.21	0.5	0.8	0.3	0.01

4 mmHg	A* (N/m)	B	σ (deg)	Rrms (N/m)	r^2
1	15.67	8.4	14.4	5.1	0.995
2	5.18	12.0	14.6	4.4	0.982
3	6.74	9.6	15.7	5.6	0.966
4	10.72	10.3	14.7	7.1	0.990
5	7.92	7.1	16.5	6.7	0.976
6	13.08	6.7	18.1	8.1	0.976
7	10.68	9.9	16.6	6.5	0.979
8	30.10	16.3	15.2	6.7	0.995
9	24.92	17.7	10.1	5.2	0.984
10	6.23	10.4	13.9	6.7	0.987
11	8.62	18.1	14.0	5.5	0.993
mean	12.71	11.5	14.9	6.1	0.98
sem	2.42	1.2	0.6	0.3	0.00

in Table 1. The fits to data from the fixed samples were slightly better than for the native tissue. This was due to the relatively sharp transition between the ''low modulus'' and ''high modulus'' regions of the native tissue stress–strain curves (Fig. 2) compared to the chosen exponential fiber material law (Eq. (2)).

An important feature of the structural model was its ability to account for small misalignments (<10 deg) of the specimen with the biaxial testing device axes. To demonstrate the importance of alignment compensation, we performed simulations using representative values for A^*, B, and σ from the 4 mmHg fixed valve database (Table 1) and values of μ ranging from 0 to 30 deg. Even when μ was as small as 10 deg, the effects of the misalignment on the stress–strain behavior were pronounced (Fig. 4). Thus, when working with highly aligned structures such as the AV cusp, accurate specimen alignment to the test device axes can become critical unless the misalignment is measured and accounted for.

Effective Fiber Stress–Strain Response. The numerical averages of A^*, B, and σ for each group are listed in Table 1. However, due to the nonlinearity of the effective fiber stress–strain law (Eq. (2)), the parameters A^* and B were not directly compared between groups (see Discussion). Rather, Eq. (2) was used to calculate the effective fiber stress–strain curves in 2 N/m increments from 0 to 60 N/m for each specimen using the A^* and

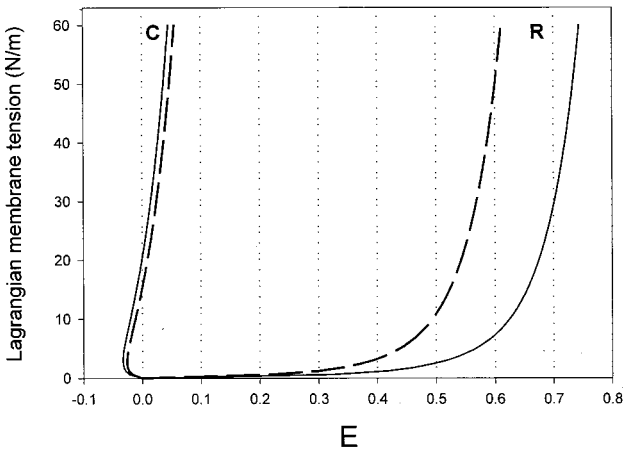

Fig. 4 Simulation of the effect of misalignment of the biaxial test specimen to testing axes by setting μ=10 deg, demonstrating a large change in peak extensibilities, especially in the radial direction. This result underscores the need for complete deformation state analysis and compensation of small misalignments when studying highly aligned fibrous tissues such as the AV cusp.

B values in Table 1. The individual fiber stress–strain curves were then averaged to determine mean fiber stress–strain curves for each group (Fig. 5).

The results demonstrated that, although all curves are exponential by definition (Eq. (2)), the fibers from the native group were more compliant at low stresses and stiffer at high stresses than the fibers from either of the fixed groups (Fig. 5). The effective fiber extensibility of the zero-pressure fixed samples was not significantly different than for the native samples, whereas the fiber extensibility of the 4 mmHg fixed samples was markedly lower.

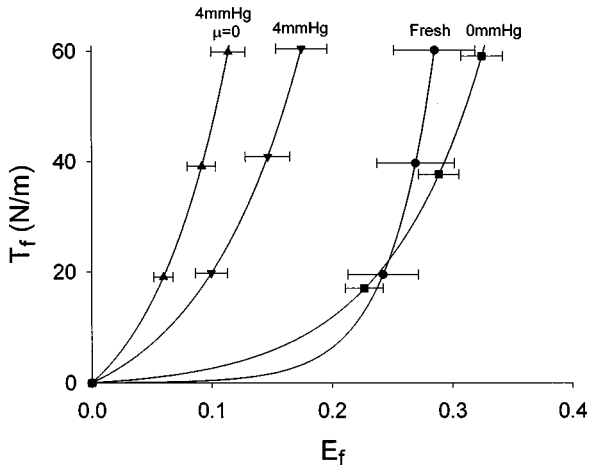

Fig. 5 Effective fiber stress–strain curves calculated using Eq. (2) from 0 to 60 N/m and the A^* and B values in Table 1. Native and 0 mmHg fixed tissue had relatively similar responses, whereas the loss of collagen fiber crimp by the application pressure during glutaraldehyde treatment clearly decreased the effective fiber compliance in the 4 mmHg fixed group. Also shown is the result for the 4 mmHg specimens re-analyzed with μ=0. Although smaller than the pressure fixation effects, this left shift in the stress–strain curve demonstrates how inaccuracies in the parameter values can be introduced when small misalignments are not accounted for when studying highly aligned fibrous tissues.

The characteristic gradual upward sloping of the effective fiber stress–strain curve was the same for the zero- and low-pressure fixed tissues.

To investigate the sensitivity of the parameters of the effective fiber stress–strain curves on the misalignment (measured deviation of μ from 0 deg), we reanalyzed the biaxial data by setting $\mu=0$ deg for the 4 mmHg pressure fixed group (Fig. 5). The fiber stress–strain curve was shifted to the left, indicating that the effective fiber stiffness can be underestimated if misalignment effects are neglected, although the shift was small relative to the difference between the zero- and low-pressure fixed groups. This result underscores the need to perform the complete deformation state analysis when studying highly aligned tissues such as the AV cusp.

While the A^* and B values cannot be directly compared between groups, the third structural model parameter σ can be. Values for σ (Table 1) indicated that the mean native specimen σ values were lower by ~4 deg and statistically different from both fixed tissue specimen groups ($p<0.01$). The fixed tissue groups were not different from each other ($p<0.01$). Overall, chemical treatment appears to increase the values for σ, with no apparent effects of pressure state during fixation within a pressure range of 0 to 4 mmHg.

Constitutive Model Parametric Analysis. Two distinguishing aspects of the AV cusp biaxial behavior, namely the extreme mechanical anisotropy and the strong mechanical coupling between the axes, can be explained by the angular distribution of fibers. The anisotropy of the tissue increases as σ decreases, so that the fiber distribution becomes more ''tight.'' To demonstrate this effect more clearly, we generated simulations under equibiaxial loading for a given set of A^* and B values by letting σ vary (Fig. 6). These simulations indicate that the value of σ is the primary determinant of the biaxial stress–strain response, as shown for (*a*) nearly random ($\sigma=90$ deg), (*b*) moderately anisotropic ($\sigma=35$ deg, similar to bovine pericardium), (*c*) highly anisotropic, including contraction along one axis ($\sigma=20$ deg), and (*d*) extremely anisotropic ($\sigma=10$ deg).

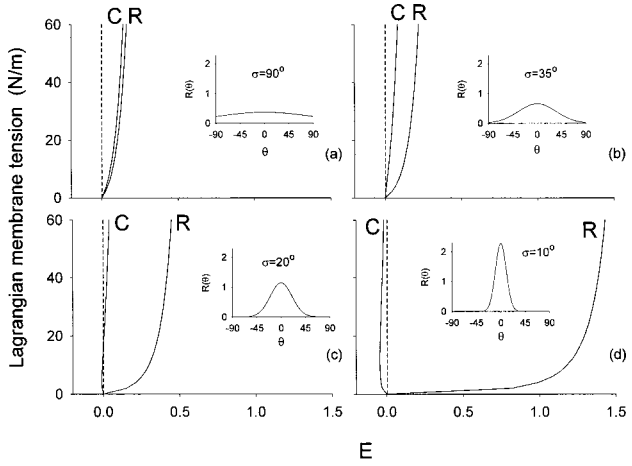

Fig. 6 Simulations using the structural model of the effect of σ on the equibiaxial stress–strain behavior. The insets provide a graphic representation of the fiber probability density distribution for each σ value: (*a*) $\sigma=90$ deg, approximately isotropic, (*b*) $\sigma=35$ deg, response qualitatively similar to bovine pericardium, (*c*) $\sigma=20$ deg, the circumferential strains are negative at low equibiaxial tensions, and (*d*) $\sigma=10$ deg, the material behavior is highly anisotropic. The dotted lines indicating zero strain are included to highlight ability of the model to simulate the crossover to negative strain observed in the pressure fixed cusps subjected to equibiaxial tension.

Discussion

This work represents the first constitutive model for the biaxial behavior of the native and glutaraldehyde-treated aortic valve cusp. The model presented herein is based on the fiber architecture of the AV cusp and is capable of predicting the complex biaxial strain response of porcine cusped material in the native, zero-pressure treated, and low-pressure treated states using only three parameters. The model is valid over an extremely wide range of loading conditions, which allow application to the physiological range and potentially nonphysiologic loading that may occur during PBHV failure.

The model simulated the response to all seven biaxial loading protocols from predominantly circumferential, to equibiaxial, to predominantly radial loading. Multiple stress protocols were employed to obtain ''true'' material parameters valid over a wide range of loading states. The use of multiple protocols also avoided the harmful effects of collinearities inherent in biaxial testing (see Choi and Vito [35] for an excellent discussion). The qualitative fit to the data is excellent, considering the ranges of stresses and strains and the complexity of response. The quantitative ''goodness of fit'' was comparable to phenomenological models of other tissues [19,35,36,38].

Strictly speaking, a biaxial strain state is not absolutely required for parameter determination of the structural model (Eq. (6)). However, the experimental data used in the current work was derived using biaxial data from Part I [12], which was performed to mimic the in vivo (diastolic) loading state. Since any model must demonstrate that it can simulate the in vivo response, testing the model against biaxial data is essential. This is especially important for tissues, such as the aortic valve cusp, where fibers undergo large rotations. Uniaxial testing tends to induce abnormally large, nonphysiological fiber rotations, since one edge is stress-free and a thin specimen is usually used. Parameters derived from uniaxial testing could potentially be incorrect due to these effects, thus necessitating biaxial testing.

As with all nonlinear constitutive models, the parameter values are generally dependent upon the particular choice of loading states (e.g., choice of peak load) and the reference configuration (e.g., magnitude of tare load) [35,39,40]. However, unlike many phenomenological models, the parameter values changed predictably and only slightly when the test conditions were changed. For example, computing the strains relative to a preloaded and preconditioned reference configuration can make a tissue appear stiffer and less extensible than using the unconstrained and unloaded reference configuration. Even small adjustments in the tare load may result in large changes in the parameter values [36]. In the AV cusp, use of a preloaded reference state reduced radial strains substantially more than the circumferential strains, which in turn produced more qualitatively isotropic behavior. As expected, when this new data set was fit, the effective fiber distribution was broader and the effective fiber stiffness was greater (i.e., A^*, B, and σ were all slightly larger).

The constitutive model simulations (Fig. 6) clearly indicate that the structural model captures the effects of the large fiber rotations under biaxial loading. In Part I, we hypothesized that these large rotations produced contraction along the circumferential direction and coupling between the axes (Part I, Fig. 7). These effects are clearly reproduced by the structural model when σ is ~20 deg or less (Fig. 6). Thus, much of the complex in-plane biaxial behavior of the AV cusp can be explained by the large strain effects of a tissue composed fibers with a tight angular distribution.

Alternative Constitutive Models. Other constitutive models for planar tissues are typically of the Fung-type (e.g., $W=(c/2)e^Q$, where $Q=0.5\ c_{ijkl}E_{ij}E_{kl}$), as recently used by Sacks [30] or assume transverse isotropy as used for myocardium [17,36,41] and mitral valve tissue [19]. While a comprehensive test of all relations is beyond the scope of this study, it is informative to demonstrate the utility of a structural approach in mini-

mizing the number of parameters necessary to model the in-plane behavior of the cusp. In the case of the Fung type, a three parameter version would be:

$$W = \frac{c}{2}[\exp(A_1 E_{11}^2 + A_2 E_{22}^2) - 1] \tag{9}$$

Using $S_{ij} = \partial W / \partial E_{ij}$, we attempted to fit this to the porcine aortic valve data. Not surprisingly, the resulting equations could not fit the data well due, in part, to the lack of shear and coupling terms. Especially evident was the inability to simulate negative strains. Expanding the number of terms in Q would obviously improve the fit, but would also increase the complexity of the nonlinear optimization and may lead to overparameterization. Alternatively, since the tests were run under tension control, use of a complementary strain energy density function would also appear to be an attractive approach. However, regardless of the particular approach used, it is unlikely that a simple analytical function can be found that reproduces the complex behavior with only three parameters. In addition to minimizing the number of parameters, the strength of the current structural approach is underscored by the insight given into the mechanics of the aortic valve cusp (e.g., fiber rotations allowing for the large radial strains).

Relation to Physiologic Loading State. Naturally, we must question what the actual physiologic loading states of the native AV and PBHV cusps are, and how well the current constitutive model simulates those states. Current finite element models of the aortic valve are quite limited (e.g., do not utilize realistic constitutive models), and while we have used these models to estimate the upper stress bounds, a detailed stress/strain history of valvular tissue from FEM simulations is not currently available. As stated in Part I of this work [12], the two major considerations for our choice of biaxial protocols were (1) generation of stress–strain data to encompass the complete in-plane response, and (2) coverage of the estimated physiological loading/range. Of these two, we chose the former since it should encompass the physiological range as well as nonphysiological loads that increase the validity of the fit material parameters. Since the current model parameters were determined utilizing an extremely wide range of loading protocols, we believe that these parameters are valid for simulating the in vivo stress–strain response of both native and bioprosthetic valves. Strain analysis from biplane markers implanted on the surface of native and bioprosthetic heart valves is currently underway in our laboratory and should allow us to check the range of our biaxial strains with a close approximation to the in vivo strain history of the valve cusp [42].

Mechanics of the Native AV and PBHV Cusp. The fact that the constitutive model works well with only three parameters is a direct result of its structural foundation. It appears that many planar collagenous tissues exhibit characteristic behavior that can, as a first approximation, be explained by a single population of fibers that have a nonlinear stress–strain response. The model highlights the importance of the angular fiber distribution in generating anisotropy and coupling between the axes in these tissues. In particular, previously inexplicable negative strains observed in equibiaxial tension experiments on pressure fixed AV cusps [9] can now be explained by the axial coupling, a direct consequence of the small splay of the fibers. Thus, in addition to the predictive capability requisite of any constitutive relation, structural models can potentially be used to separate the effects of the structural arrangement of the constituents from the properties of the constituents themselves, providing insight into the linkage between the ''organ-level'' stresses and the local micro-mechanical events.

For example, we examined the effects of zero- and low-pressure fixation on the effective fiber stress–strain relationship independent of variations in the angular distribution of fibers between individual samples. The effective fiber properties were substantially different between the zero- and low-pressure fixed groups (Fig. 5). The concomitant increase in σ due to chemical fixation, although statistically significant (Table 1), was small and likely secondary to the larger alterations in the effective fiber stress–strain relation. Changes in the mechanical behavior of cusps following pressure fixation have long been noted and have generally been attributed to removal of much of the native collagen fiber crimp during fixation [6–8]. Our data support this conclusion. The relatively compliant behavior of the native and low-pressure groups, as seen in the effective fiber stress–strain curves at low stress levels, is consistent with tissues with large crimp amplitude and little resistance to fiber straightening (Figs. 2 and 5). This result is also consistent with our previous finding that the large undulations of the collagen fibers are virtually eliminated when the transvalvular pressure is only 4 mmHg [15].

In related structural modeling work, we were able to use SALS data to obtain the angular distribution of collagen fibers directly [20,21,43]. This was due to the fact that, unlike in the aortic valve, bovine pericardium has a simpler structure (e.g., no dense chordal structures), where all collagen fibers appear to equally withstand loading. For chemically treated bovine pericardium, we found that chemical fixation not only altered the effective fiber stress–strain relationship but also added a second, isotropic material phase [20,21]. Interestingly, the mechanical effect of this second, isotropic material phase could not be simulated by simply increasing σ. For the AV cusp, no secondary isotropic phase was required to obtain accurate fits to the data. While the cause of this is not entirely clear at this time, the extreme stiffness of AV cuspal fibers suggests that the contribution of a second material phase would be negligible in comparison. It is also possible that the nature of the chemical bonding process in the two tissues is different, potentially due in part to their different structures. In any case, the effects of chemical fixation on tissue mechanical behavior are complex and require further attention.

Parameter Interpretation. As with any nonlinear relationship, it is not meaningful to compare the individual A^* and B parameter values between groups or to ascribe to them any direct physical meaning. However, information regarding the mechanisms underlying the nonlinearity of the effective fiber stress–strain relationship is available from the structure of the cusp. For uniaxially loaded structures such as tendon and ligament, the distribution of crimp extinction strains has been used to explain the nonlinear form of the stress–strain curve (e.g., [23,44–47]). In contrast, for the valve cusp higher order structures such as the macroscopic radial corrugation, the dense fiber bundles of the fibrosa, and finer collagen fiber network of the ventricularis exist and may play an important role in fiber-level mechanics. While previous attempts to accurately quantify the crimp in the AV cusp have produced variable results [8], more quantitative morphological work on the AV cuspal structure is clearly required to more fully develop the effective fiber stress–strain model.

Although the structural model parameter σ has a direct physical meaning (corresponding to the angular distribution of collagen fibers), physical interpretation within the context of the assumptions of the constitutive model must be interpreted with caution. The σ values determined by the optimization routine ranged from approximately 10 to 20 deg, which were substantially lower than the ~35 deg angular splay values measured using SALS [15]. This discrepancy is most likely due to the fact that in SALS the measured σ values include the optical scattering of all fibers through the multiple layers of the cusps, including those that contribute negligibly to the in-plane biaxial response.

To investigate this hypothesis, we decomposed the SALS data from the AV cusp into two separate Gaussian distributions using our previous methods [48] (Fig. 7). We believe that the resulting tight distribution ($\sigma_1 = 16$ deg) corresponds to our effective fiber population (i.e., the collagen fiber bundles in the fibrosa), and the broader distribution ($\sigma_2 = 44$ deg) represents finer collagen and elastin fibers of the fibrosa and ventricularis. Next, we utilized the modified $R(\theta)$ in the structural model to include two separate fiber populations. When fit to the experimental data, the contribution of

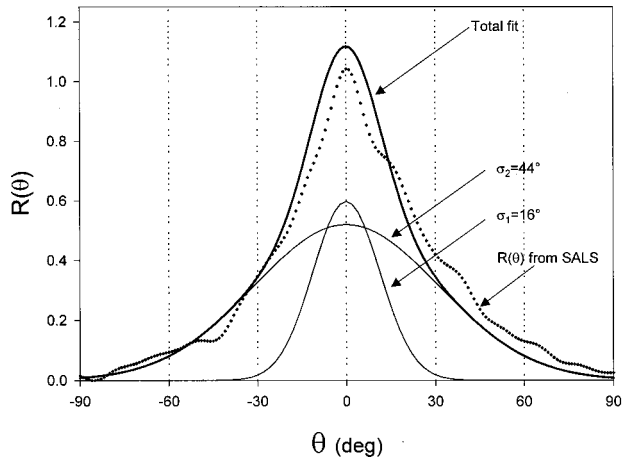

Fig. 7 A representative $R(\theta)$ distribution from an AV cusp fit to a dual Gaussian distribution using the methods of Sacks and Chuong [48]. Here, the AV cusp fiber orientation distribution was principally composed of a highly aligned population ($\sigma_1 = 16$ deg) and a broader distribution ($\sigma_2 = 44$ deg). Although the fibers of both populations contribute to $R(\theta)$, the mechanical contribution of the fibers belonging to σ_2 was negligible, supporting our assumption that the in-plane biaxial response can be modeled by a single highly aligned fiber population within the cusp.

the effective fiber stress–strain response for the second fiber population (σ_2) was negligible compared to the primary fiber population (σ_1). This result supports our hypothesis that the predominant role of the large fibrosa collagen bundles in supporting the majority of the planar tensile loads, and that the more uniformly distributed fibers have comparatively little affect on the planar biaxial response. The small increase in σ with GL treatment, regardless of pressure (Table 1), may be indicative of a cross-linking of fibers from ''secondary'' populations to the mechanically dominant fiber population. This binding may allow these fibers to play a greater role in the tensile properties of the fixed tissues than the native tissues. This effect appears to be of lesser importance mechanically compared to changes in the fiber properties themselves.

Limitations. The constitutive model fit data from fixed tissue slightly better than for native tissue. This may be due, in part, to the fact that the effective fiber stress–strain curves for chemically treated tissues are smoother (have no abrupt transitions, Fig. 2) and can be fit better by Eq. (1). Other forms of the effective fiber stress–strain relationship may be necessary to improve the fit for native tissues. Data from a few samples were skewed by pronounced asymmetry of the collagen fiber architecture outside of the region delimited by the graphite markers. Use of multiple marker regions and a finite element method (e.g., [49]) could potentially solve this problem but would require extensive computational work. As discussed in Part I of this work [12], due to the heterogeneity of the cusp model, parameters are valid only for the region delimited by the deformation markers (i.e., the lower belly region).

A further impediment to proper fitting of the data for some samples was uneven flattening of the sample from its curved unconstrained configuration. Although the unloaded cusp is roughly a shallow spherical cap and can deform nonuniformly when flattened, we still consider the unloaded slightly curved state to be the most valid reference configuration. Retaining data from the low-stress region of the stress–strain curve by using the unconstrained reference configuration is even more important in the AV cusp than other soft tissues due to the physiological relevance of the unloaded state (i.e., systole). Furthermore, in addition to large differences in stiffness at low loads between native and pressure-fixed tissues [50], there are also large differences in the stiffness between radial and circumferential axes at low loads. Disregarding this information can lead to nonsensical interpretation of the data, such as increased compliance following chemical fixation.

Summary. We have formulated the first constitutive model to describe the complete measured planar biaxial stress–strain of the native and glutaraldehyde-treated aortic valve cusp using a structurally guided approach. The model was able to simulate a wide range of in-plane mechanical behavior and account for misalignment of the test specimen, which increased our confidence in the parameter values. Compared to past implementations of structural models, the parameter values presented herein represent a relatively large and complete set of data (30 samples, each with seven loading protocols). Although we assumed a simplified cuspal structure in the formulation of the model, the structural approach highlighted the importance of the angular orientation of the fibers in determining the complex anisotropic mechanical behavior of the tissue. Knowledge derived from this model may aid in the development of more durable bioprosthetic heart valves, and potentially lay the groundwork for the design of tissue engineered scaffolds for replacement heart valves that mimic the native aortic valve cusp.

Acknowledgments

The support of the American Heart Association, Florida Affiliate, is gratefully acknowledged. The authors would like to also thank St. Jude Medical for supplying the heart valves.

Appendix 1

Calculation of the Deformation Components From the Marker Positions. For the two-dimensional deformation of the tissue to be uniquely determined, the Cartesian coordinates (x_1, x_2) of a point on the undeformed surface of the tissue, and the coordinates of the same point following deformation (y_1, y_2) are uniquely related to each other by:

$$y_i = y_i(x_1,\ x_2) \tag{A1}$$

where x_i and y_i are unique and continuously differentiable. For the case where the loading produces general planar deformation with shear, the relationship between the initial and final Cartesian coordinates is:

$$y_i = F_{ij} x_j \tag{A2}$$

F is the deformation gradient,

$$F_{ij} = \begin{bmatrix} \lambda_1 & \kappa_1 \\ \kappa_2 & \lambda_2 \end{bmatrix} \tag{A3}$$

where the λ_i's are the axial stretch ratios and κ_i are the shear terms. Note that when $\kappa_1 \neq \kappa_2$, there is rigid body rotation during deformation. The angle of rigid body rotation can be determined using polar decomposition as discussed below.

The deformation gradient was computed from the experimentally measured marker displacements, using a four-node isoparametric finite element to compute the necessary gradient terms. This method was developed by Hoffman and Grigg [51], and later refined by Humphrey et al. [52]. The interested reader is referred to these works for details of the computations involved.

Appendix 2

Calculation of the Preferred Fiber Direction Relative to the Biaxial Test Axes (i.e., Misalignment). Misalignment between the sample material axes and the biaxial test axes was determined by measuring the preferred fiber direction using SALS. The difference in sample mounting orientation between the biaxial device and the SALS device was removed by subtracting the rigid body rotation (θ_{rb}) from the preferred fiber direction. To calculate θ_{rb},

the SALS marker positions were considered to be the positions of the biaxial markers following a general two-dimensional deformation described by the deformation gradient, F, computed as described in Appendix 1. Polar decomposition was employed to calculate the rotation of the specimen between the biaxial and SALS marker positions using the following equation:

$$F_{ij} = \frac{\partial x_i}{\partial X_j} = D_{ik} R_{kj} \tag{A4}$$

In this case, the ''stretch'' tensor, D_{ij}, is simply a scale factor between the biaxial device camera and the SALS device camera. R_{ij} is the orthogonal rotation tensor:

$$R = \begin{bmatrix} \cos\theta_{rb} & \sin\theta_{rb} \\ -\sin\theta_{rb} & \cos\theta_{rb} \end{bmatrix} \tag{A5}$$

The angle θ_{rb} is obtained by solving for R_{ij} from Eq. (*A*4).

References

[1] Krucinski, S., Vesely, I., Dokainish, M. A., and Campbell, G., 1993, ''Numerical Simulation of Leaflet Flexure in Bioprosthetic Valves Mounted on Rigid and Expansile Stents,'' J. Biomech., **26**, pp. 929–943.

[2] Christie, C. W., and Medland, I. C., 1982, ''A Non-linear Finite Element Stress Analysis of Bioprosthetic Heart Valve,'' *Finite Element in Biomechanics*, Gallagher, R. H., Simon, B. R., Johnson, P. C., and Gross, J. F., eds., Chichester, Wiley, pp. 153–179.

[3] Lee, J. M., Courtman, D. W., and Boughner, D. R., 1984, ''The Glutaraldehyde-Stabilized Porcine Aortic Valve Xenograft. I. Tensile Viscoelastic Properties of the Fresh Leaflet Material,'' J. Biomed. Mater. Res., **18**, pp. 61–77.

[4] Lee, J. M., Boughner, D. R., and Courtman, D. W., 1984, ''The Glutaraldehyde-Stabilized Porcine Aortic Valve Xenograft. II. Effect of Fixation With or Without Pressure on the Tensile Viscoelastic Properties of the Leaflet Material,'' J. Biomed. Mater. Res., **18**, pp. 79–98.

[5] Vesely, I., and Noseworthy, R., 1992, ''Micromechanics of the Fibrosa and the Ventricularis in Aortic Valve Leaflets,'' J. Biomech., **25**, pp. 101–113.

[6] Broom, N., and Christie, G. W., 1982, ''The Structure/Function Relationship of Fresh and Gluteraldehyde-Fixed Aortic Valve Leaflets,'' *Cardiac Bioprosthesis*, Cohn, L. H., and Gallucci, V., eds., Yorke Medical Books, New York, pp. 477–491.

[7] Christie, G. W., 1992, ''Anatomy of Aortic Heart Valve Leaflets: The Influence of Glutaraldehyde Fixation on Function,'' Eur. J. Cardio-Thoracic Surg., **6**, pp. S25–S33.

[8] Hilbert, S., Barrick, M., and Ferrans, V., 1990, ''Porcine Aortic Valve Bioprosthesis: A Morphologic Comparison of the Effects of Fixation Pressure,'' J. Biomed. Mater. Res., **24**, pp. 773–787.

[9] Mayne, A. S. D., Christie, G. W., Smaill, B. H., Hunter, P. J., and Barratt-Boyes, B. G., 1989, ''An Assessment of the Mechanical Properties of Leaflets From Four Second-Generation Porcine Bioprosthesis With Biaxial Testing Techniques,'' J. Thorac. Cardiovasc. Surg., **98**, pp. 170–180.

[10] Christie, G. W., and Barratt-Boyes, B. G., 1995, ''Age-Dependent Changes in the Radial Stretch of Human Aortic Valve Leaflets Determined by Biaxial Stretching,'' Ann. Thoracic Surg., **60**, pp. S156–S159.

[11] Brossollet, L. J., and Vito, R. P., 1996, ''A New Approach to Mechanical Testing and Modeling of Biological Tissues, With Application to Blood Vessels,'' ASME J. Biomech. Eng., **118**, pp. 433–439.

[12] Billiar, K., and Sacks, M., 2000, ''Biaxial Mechanical Properties of Fresh and Glutaraldehyde Treated Porcine Aortic Valve Cusps: Part I—Experimental Findings,'' ASME J. Biomech. Eng., **122**, pp. 23–30.

[13] Rousseau, E. P. M., Sauren, A. A. H. J., Van Hout, M. C., and Van Steenhoven, A. A., 1983, ''Elastic and Viscoelastic Material Behaviour of Fresh and Glutaraldehyde-Treated Porcine Aortic Valve Tissues,'' J. Biomech., **16**, pp. 339–348.

[14] Sauren, A., van Hout, M., van Steenhoven, A., Veldpaus, F., and Janssen, J., 1983, ''The Mechanical Properties of Porcine Aortic Valve Tissues,'' J. Biomech., **16**, pp. 327–337.

[15] Sacks, M. S., Smith, D. B., and Hiester, E. D., 1998, ''The Aortic Valve Microstructure: Effects of Trans-Valvular Pressure,'' J. Biomed. Mater. Res., **41**, pp. 131–141.

[16] Fung, Y. C., 1993, *Biomechanics: Mechanical Properties of Living Tissues*, Springer-Verlag, New York.

[17] Humphrey, J. D., Strumpf, R. K., and Yin, F. C. P., 1990, ''Determination of a Constitutive Relation for Passive Myocardium: I. A New Functional Form,'' ASME J. Biomech. Eng., **112**, pp. 333–339.

[18] Humphrey, J. D., Strumpf, R. K., and Yin, F. C. P., 1992, ''A Constitutive Theory for Biomembranes: Application to Epicardial Mechanics,'' ASME J. Biomech. Eng., **114**, pp. 461–466.

[19] May-Newman, K., and Yin, F. C. P., 1998, ''A Constitutive Law for Mitral Valve Tissue,'' ASME J. Biomech. Eng., **120**, pp. 38–47.

[20] Sacks, M. S., 2000, ''A Structural Constitutive Model for Chemically Treated Planar Connective Tissues Under Biaxial Loading,'' Comput. Mech., in press.

[21] Sacks, M., 1999, ''A Structural Model for Chemically Treated Soft Tissues,'' *1999 Advances in Bioengineering*, ASME BED-Vol. 43, pp. 101–102.

[22] Lanir, Y., 1983, ''Constitutive Equations for Fibrous Connective Tissues,'' J. Biomech., **16**, pp. 1–12.

[23] Lanir, Y., 1979, ''A Structural Theory for the Homogeneous Biaxial Stress–Strain Relationships in Flat Collageneous Tissues,'' J. Biomech., **12**, pp. 423–436.

[24] Harkness, M., and Harkness, R., 1959, ''Effect of Enzymes on Mechanical Properties of Tissues,'' Nature (London), **183**, pp. 1821–1822.

[25] Humphrey, J. D., and Yin, F. C. P., 1987, ''A New Constitutive Formulation for Characterizing the Mechanical Behavior of Soft Tissues,'' Biophys. J., **52**, pp. 563–570.

[26] Vesely, I., Boughner, D. R., and Leeson-Dietrich, J., 1995, ''Bioprosthetic Valve Tissue Viscoelasticity: Implications on Accelerated Pulse Duplicator Testing,'' Ann. Thoracic Surg., **60**, pp. S379–S383.

[27] Nielsen, P. M. F., Hunter, P. J., and Smaill, B. H., 1991, ''Biaxial Testing of Membrane Biomaterials: Testing Equipment and Procedures,'' ASME J. Biomech. Eng., **113**, pp. 295–300.

[28] Thubrikar, M., 1990, *The Aortic Valve*, CRC, Boca Raton.

[29] Billiar, K. L., and Sacks, M. S., 1997, ''A Method to Quantify the Fiber Kinematics of Planar Tissues Under Biaxial Stretch,'' J. Biomech., **30**, 753–756.

[30] Sacks, M. S., 1999, ''A Method for Planar Biaxial Testing That Includes In-Plane Shear,'' ASME J. Biomech. Eng., **121**, pp. 551–555.

[31] Lanir, Y., Lichtenstein, O., and Imanuel, O., 1996, ''Optimal Design of Biaxial Tests for Structural Material Characterization of Flat Tissues,'' ASME J. Biomech. Eng., **118**, pp. 41–47.

[32] Zioupos, P., and Barbenel, J. C., 1994, ''Mechanics of Native Bovine Pericardium: II. A Structure Based Model for the Anisotropic Mechanical Behavior of the Tissue,'' Biomaterials, **15**, pp. 374–382.

[33] Spencer, A. J. M., 1980, *Continuum Mechanics*, Longman Scientific & Technical, New York.

[34] Press, W. H., Flannery, B. P., Teukolsky, S. A., and Vetterling, W. T., 1988, *Numerical Recipes in C*, Cambridge University Press, Cambridge.

[35] Choi, H. S., and Vito, R. P., 1990, ''Two Dimensional Stress–Strain Relationship for Canine Pericardium,'' ASME J. Biomech. Eng., **112**, pp. 153–159.

[36] Humphrey, J. D., Strumpf, R. K., and Yin, F. C. P., 1990, ''Determination of a Constitutive Relation for Passive Myocardium: II—Parameter Estimation,'' ASME J. Biomech. Eng., **112**, pp. 340–346.

[37] Billiar, K., 1998, ''A Structurally Guided Constitutive Model for Aortic Valve Bioprostheses: Effects of Glutaraldehyde Treatment and Mechanical Fatigue,'' Ph.D. Dissertation in Bioengineering, University of Pennsylvania, Philadelphia.

[38] Fung, Y. C., Fronek, K., and Patitucci, P., 1979, ''Pseudoelasticity of Arteries of the Choice of Its Mathematical Expression,'' Am. J. Physiol., **237**, pp. H620–H631.

[39] Yin, F. C. P., Chew, P. H., and Zeger, S. L., 1986, ''An Approach to Quantification of Biaxial Tissue Stress–Strain Data,'' J. Biomech., **19**, pp. 27–37.

[40] Fung, Y. C., 1990, *Biomechanics: Motion, Flow, Stress, and Growth*, Springer-Verlag, New York.

[41] Sacks, M. S., and Chuong, C. J., 1993, ''A Constitutive Relation for Passive Right-Ventricular Free Wall Myocardium,'' J. Biomech., **26**, pp. 1341–1345.

[42] Sacks, M. S., Smith, D. B., Thornton, M., and Iyengar, A. K. S., 1999, ''Real Time Deformation of the Bioprosthetic Heart Valve,'' *Proc. First Joint BMES/EMBS Conference*, Atlanta, GA, IEEE, p. 173.

[43] Sacks, M. S., 1999, ''A Structural Constitutive Model for Pericardium That Utilizes SALS-Derived Fiber Orientation Information,'' ASME J. Biomech. Eng., submitted.

[44] Hurschler, C., Loitz-Ramage, B., and Vanderby, R., 1997, ''A Structurally Based Stress–Stretch Relationship For Tendon and Ligament,'' ASME J. Biomech. Eng., **119**, pp. 392–399.

[45] Comninou, M., and Yannas, I. V., 1976, ''Dependence of Stress–Strain Nonlinearity of Connective Tissues on the Geometry of Collagen Fibers,'' J. Biomech., **9**, pp. 427–433.

[46] Decraemer, W. F., Maes, M. A., and Vanhuyse, V. J., 1980, ''An Elastic Stress–Strain Relation for Soft Biological Tissues Based on a Structural Model,'' J. Biomech., **13**, pp. 463–468.

[47] Shoemaker, P. A., Schneider, D., Lee, M. C., and Fung, Y. C., 1986, ''A Constitutive Model for Two-Dimensional Soft Tissues and Its Application to Experimental Data,'' J. Biomech., **19**, pp. 695–702.

[48] Sacks, M. S., and Chuong, C. J., 1992, ''Characterization of Collagen Fiber Architecture in the Canine Central Tendon,'' ASME J. Biomech. Eng., **114**, pp. 183–190.

[49] Oomens, C. W. J., Ratingen, M. R. V., Janssen, J. D., Kok, J. J., and Hendriks, M. A. N., 1993, ''A Numerical–Experimental Method for a Mechanical Characterization of Biological Materials,'' J. Biomech., **26**, pp. 617–621.

[50] Trowbridge, E. A., and Crofts, C. E., 1986, ''The Standardization Gauge Length: Its Influence on the Relative Extensibility of Natural and Chemically Modified Pericardium,'' J. Biomech., **19**, pp. 1023–1033.

[51] Hoffman, A. H., and Grigg, P., 1984, ''A Method for Measuring Strains in Soft Tissue,'' J. Biomech., **10**, pp. 795–800.

[52] Humphrey, J., Vawter, D., and Vito, R., 1987, ''Quantification of Strains in Biaxially Tested Soft Tissues,'' J. Biomech., **20**, pp. 59–65.